Modeling and Simulation for a Nano-Photonic Quantum Dot Waveguide Fabricated by DNA-Directed Self-Assembly

Chia-Jean Wang, *Student Member, IEEE*, Lih Y. Lin, *Senior Member, IEEE*, and Babak A. Parviz, *Member, IEEE*

Abstract—We propose a nano-photonic waveguide structure by DNA-directed self-assembled fabrication. In this paper, we focus on the study of quantum dot (QD) behavior under optical stimulation in terms of gain, absorption, and emission characteristics. Both continuous wave (CW) and pulsed operations are considered and the results are compared utilizing the CdSe/ZnS and $In_{0.47}Ga_{0.53}$ As/InP core/shell material systems. Gain coefficients reach optima at pump powers of 0.055 and 0.05 nW for the former and 0.11 and 0.019 μW for the latter in 100 ps pulsed and CW cases, respectively. Due to their unique properties and size, QDs provide a means to create integrated photonic circuits on the nanoscale. Accordingly, the optical propagation of a QD waveguide array in a single line formation is simulated and demonstrates a viable subdiffraction limit optical energy transfer for high coupling coefficient between adjacent QDs. A proposed fabrication process by DNA-directed self-assembly is also described.

Index Terms—Nano-scale photonic waveguide, optical pumping, quantum dot (QD) modeling, subdiffraction limit.

I. INTRODUCTION

THE QUANTUM dot (QD), which has been a subject of investigation for several decades, is at the crux of current technological efforts. First developed as the logical successor to quantum well and then quantum film lasing structures [1]–[3] with superior optical properties due to higher degrees of confinement, the QD is finding applications in many fields, such as optical labels in biomedicine [4], [5], in addition to many photonic devices [6], [7]. The nanosized device garners wide interest due to its position at the gateway between the micrometer level over which we commonly exert control and the molecular level manipulation which we hope to fully achieve.

The composition of a QD can be tailored for compatibility with respect to its usage. In a core/shell structure, the maximum number of supported electron and hole states is defined by the energy gap difference between the core and shell material, which forms a potential well. The wavelengths of photons emitted by exciton recombination, which is chiefly determined by the energy bandgap of the core compound, is modified by varying the core diameter or effective length, such that a larger dimension corresponds to lower quantum energies between the conduction or valence band edge and electron or hole energy levels. The capability to tune photon emission across the infrared to ultraviolet spectrum coupled with the nanometer dimension and high optical nonlinearity properties has spawned QD innovations, such as optical transistors and switches [8], [9].

In nanophotonics, extensive effort has been spent to achieve nano-scale photonic waveguide structures for ultrahigh density photonic integrated circuits, which is the key to creating a new generation of devices that satisfy the demand for increased data transmission and processing capacity as well as enable a paradigm shift to allow the continuity of Moore's Law. Nano-scale photonic waveguides utilizing photonic crystals [10] and high-index-contrast silicon waveguides [11] have demonstrated excellent optical propagation in submicrometer scale. These approaches are constrained by the diffraction limit inherent to Heisenberg's Uncertainty Principle. To overcome this barrier, new ways of transferring electromagnetic energy below the diffraction limit in waveguiding structure have been pursued, such as negative dielectric materials and plasmonic waveguides with metal particles [12]–[15]. The chief challenge associated with these technologies is the lack of gain and plasmonic-optical conversion mechanisms.

Instead, we propose DNA-directed self-assembled QD arrays for nanophotonic waveguiding which overcome the diffraction limit and may be optically pumped to reduce loss in energy transfer [16], [17]. In this paper, the focus is on theoretical analysis that explores the QD response to optical pumping and utilizes the results to determine coupled QD behavior and optical energy transfer in a waveguide structure. Section II-A describes the device structure, and Section II-B provides a framework for the model in terms of pumping effects. Subsequently, Sections II-C and II-D detail pulsed and continuous wave (CW) mode functionality, which are implemented to contrast two core/shell QD structures, CdSe/ZnS and a reference, $In_{0.47}Ga_{0.53}As/InP$. Gain, absorption, and emission spectra along with the gain coefficient results are reported. Then, we analyze and compare the results for the two QD materials in Section II-E. Section III describes the propagation and intensity output in QD waveguides and gives the results of a waveguide of five QDs as a function of gain and the interdot coupling coefficient. A proposed fabrication process by DNA-directed self-assembly is presented in Section IV. Finally, we review the main points and elaborate on further applications in Section V.
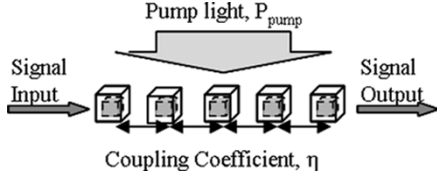
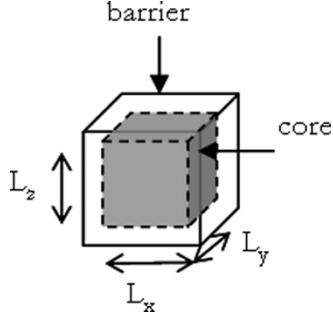Fig. 1.   Schematic drawing of self-assembled QD waveguide.

Fig. 2.   Diagram of core/shell quantum box.

II. OPTICAL GAIN MODELING

A. Device Structure

Fig. 1 shows the schematic drawing of the proposed nano-photonic QD waveguides. An array of QDs is fabricated on a silicon substrate by DNA-directed self-assembly process. The QDs are uniformly illuminated with pump light whose energy equals to the separation between the first electron state in the conduction band and the first heavy-hole state in the valence band to provide optical gain. Then, an optical signal, whose energy equals to the separation between the ground electron state and the ground heavy-hole state, creates stimulated emission in the excited QDs to produce gain. The output signal couples to the adjacent QDs through near-field optical coupling [8]. Due to this energy transfer mechanism, the optical signal can propagate through the QD array with subdiffraction limit.

B. Electrical versus Optical Pumping

On account of its origins stemming from laser development, the QD is commonly investigated using electrical pumping conditions. Consequently, gain and threshold current models are calculated with quasi-Fermi level energies E_{fc} and E_{fv}, which are directly controlled by the doping concentration or injected current [18], [19]. Given that L_x, L_y, and L_z are the lengths in each dimension of a quantum box (see Fig. 2), and E_{clmn} and E_{hlmn} are the allowed quantized electron and hole energies, respectively, the corresponding carrier densities, n and $p(\sim n)$, may be expressed as

$$
n = \sum_{\text{lmn}} \frac{2}{\left[1 + \exp\left(\frac{E_{\text{clmn}} - E_{fc}}{kT}\right)\right] L_x L_y L_z}
$$
$$
= \sum_{\text{lmn}} \frac{2 \cdot f_c(E_{\text{clmn}})}{L_x L_y L_z}, \tag{1}
$$
$$
p = \sum_{\text{lmn}} \frac{2}{\left[1 + \exp\left(\frac{E_{fv} - E_{\text{hlmn}}}{kT}\right)\right] L_x L_y L_z}
$$
$$
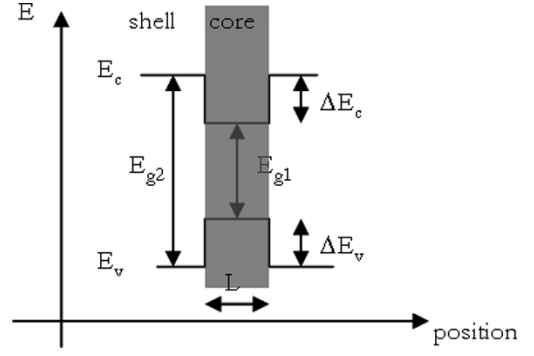= \sum_{\text{lmn}} \frac{2 \cdot (1 - f_v(E_{\text{hclmn}}))}{L_x L_y L_z} \tag{2}
$$

Fig. 3.   One-dimensional energy diagram of a QD.

TABLE I
BANDGAP AND OFFSET ENERGIES GIVEN IN ELECTRONVOLTS AT 300 K

Core/Shell	E_{g1}/E_{g2}	$\Delta E_c/\Delta E_v$
$In_{0.47}Ga_{0.53}As/InP$	0.75/1.35	0.33/0.27
CdSe/ZnS	1.7/3.68	1.03/0.95

where f_c and f_v are the corresponding Fermi functions for electrons in the conduction band and valence band. The factor of two takes into account the electron spin states per level. The summation is over all the confined energy states, which depends on the QD material and the core/shell valence and conduction band offsets (ΔE_c and ΔE_v) that enable electron and hole confinement. Together with Fig. 3, Table I shows the reference bandgap energy values and offsets for two core/shell systems, CdSe/ZnS and $In_{0.47}Ga_{0.53}As/InP$.

With the known properties, E_{fc} and E_{fv} are solved for directly and applied to find the linear absorption coefficient $\alpha(\omega)$ and linear emission coefficient $e(\omega)$ components in the QD [18]

$$
\alpha(\omega) = \frac{\omega}{n_r}\sqrt{\frac{\mu_0}{\varepsilon_0}} \sum_{\text{lmn}} \int_{E_g}^{\infty} \langle \mathbf{R}_{\text{ch}}^2 \rangle
$$
$$
\times \frac{\frac{g_{\text{ch}} f_v(E_1)[1 - f_c(E_2)]\hbar}{\tau_{\text{in}}}}{(E_{\text{ch}} - \hbar\omega)^2 + \left(\frac{\hbar}{\tau_{\text{in}}}\right)^2} dE_{\text{ch}}, \tag{3}
$$
$$
e(\omega) = \frac{\omega}{n_r}\sqrt{\frac{\mu_0}{\varepsilon_0}} \sum_{\text{lmn}} \int_{E_g}^{\infty} \langle \mathbf{R}_{\text{ch}}^2 \rangle
$$
$$
\times \frac{\frac{g_{\text{ch}} f_c(E_2)[1 - f_v(E_1)]\hbar}{\tau_{\text{in}}}}{(E_{\text{ch}} - \hbar\omega)^2 + \left(\frac{\hbar}{\tau_{\text{in}}}\right)^2} dE_{\text{ch}}. \tag{4}
$$

where $\mathbf{R}_{\text{ch}}$ is the dipole moment, n_r is the refractive index, and g_{ch} is the density of states for the QD, given as

$$
g_{\text{ch}} = \frac{2\delta(E_{\text{ch}} - E_{\text{clmn}} - E_{\text{hlmn}} - E_g)}{(L_x L_y L_z)}. \tag{5}
$$

The intraband relaxation time τ_{in} is either 0.1 or 1 ps for $In_{0.47}Ga_{0.53}As/InP$ [18] or CdSe/ZnS [20]. Equations (3) and (4) signify the rates of absorption and emission per unit
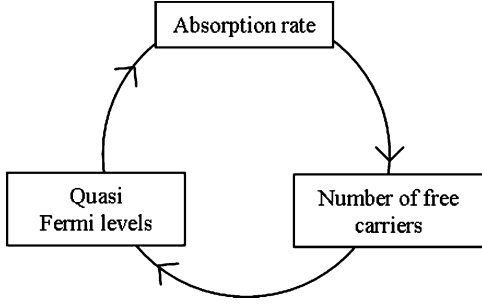
Fig. 4.   Interdependence of various parameters in an optically-pumped QD.

length with E_1 and E_2 representing the hole energy level in the valence band and the electron energy level in the conduction band, respectively. The net gain of the system is then

$$G(\omega) = e(\omega) - \alpha(\omega). \tag{6}$$

Equations (1)–(6) are consistent for both electrical and optical pumping.

However, with optical stimulation, the free carrier concentrations n and p in the QD are not linear functions of pump power, as in the case of electrical pumping. Instead, they depend on the pump power and the absorption rate, the latter of which decreases as the number of free carriers increases. As both absorption and emission rates change with the quasi-Fermi level energies and refer back to the carrier concentration, the resulting system is interconnected in a number of ways, as shown in Fig. 4. As a result, the quasi-Fermi levels must be solved in a self-consistent manner for each set of pump parameters. Furthermore, the chain of events resulting from optical stimulation differs for pulsed and CW cases and is examined as follows.

C. Pulsed Operation

In a pulsed system, laser light shines on a QD for a brief interval causing photon absorption, which then elevates electrons in the valence band to a higher quantized level in the conduction band. These electrons relax to the lowest energy level in the conduction band, and recombine with holes through stimulated emission by the input optical signal. If the pulse duration is shorter than the electron-hole recombination lifetime, as is the case in our simulation described in the following, all the excited free carriers will be utilized during stimulated emission.

The pulse light, which is fully specified by the pulse duration, Δt, magnitude in power, P_{pump}, and frequency, ω_p, along with the absorption spectrum at the pulsed frequency control the number of carriers and the resulting gain. Primarily, the pump energy must be equal to or greater than the lowest transition level, i.e., $E_g + E_{c000} + E_{h000}$, and of nonnegligible duration in order to create the dynamics necessary for population inversion. To avoid mixing with the signal light, we design the pump light energy equal to the separation between the first state in the conduction band and the heavy hole first state in the valence band, and the signal light energy equal to the separation between the ground state in the conduction band and the ground state in the valence band.

Using (1) and (2), the quasi-Fermi level energies at a given pump light of intensity $I_{\text{pump}} = P_{\text{pump}}/(L_x L_y)$ may be found

by solving a system of equations. Here, the light is incident on the x-y plane of the QD surface and z is the depth dimension. From our pump light, the resulting carrier concentration is

$$n \cong p = \frac{P_{\text{pump}}}{L_x L_y \cdot \hbar\omega_p} \Delta t \alpha(\omega_p) \tag{7}$$

which may be combined with (1) and (2) and simplified to give the total number of electrons and holes generated in the QD

$$N = \frac{P_{\text{pump}}}{\hbar\omega_p} \Delta t \alpha(\omega_p) L_z$$
$$= \sum_{\text{lmn}} \frac{2}{\left[1 + \exp\left(\frac{E_{\text{clmn}} - E_{fc}}{kT}\right)\right]}, \tag{8}$$

$$P = \frac{P_{\text{pump}}}{\hbar\omega_p} \Delta t \alpha(\omega_p) L_z$$
$$= \sum_{\text{lmn}} \frac{2}{\left[1 + \exp\left(\frac{E_{fv} - E_{\text{hlmn}}}{kT}\right)\right]}. \tag{9}$$

As expected, the number of free carriers increases with a longer pulse time and is proportional to the rate of photon absorption over the length of the device. The resulting expressions for E_{fc} and E_{fv} are subsequently applied to solve for absorption, emission, and gain from (3), (4), and (6). The procedure is repeated with any change in the pump parameters.

The pulsed case outcome as a function of signal wavelength is shown in Fig. 5 and Fig. 6 for the transition between ground state in valence band and ground state in conduction band (i.e. $E_{h000} \leftrightarrow E_{c000}$) in $10 \times 10 \times 10$ nm $In_{0.47}Ga_{0.53}As/InP$ and $5 \times 5 \times 5$ nm CdSe/ZnS core/shell QDs. The shell thickness surrounding the core is 5 nm for both cases. The corresponding peak wavelengths are at 1326 nm for the former and 594.6 nm for the latter system.

In both models, Δt is 100 ps while $E_{\text{pump}} = \hbar\omega_p$ is set at the exact difference between the first electron state and the first heavy hole state in the QD, which turns out to be 1.08 eV for $In_{0.47}Ga_{0.53}As/InP$ and 2.45 eV for CdSe/ZnS. Pump power is varied in the range of 0.001 to 1 μW and 0.001 to 1 nW, respectively, by an order of magnitude for each curve in the absorption, emission, and gain plots.

Overall, it can be observed that the gain saturates in the $In_{0.47}Ga_{0.53}As/InP$ system at higher pumping powers. Moreover, gain for the CdSe/ZnS QD is higher with a narrower peak. While the peak shape is determined by homogenous broadening, specified by the Lorentzian lineshape and the intraband relaxation time, the net result of absorption subtracted from emission depends on the Fermi levels. Therefore, the pump parameters dynamically dictate system gain.

D. CW Operation

The CW mode differs from pulsed stimulation since steady state is achieved, whereby the rates of photon absorption and emission equalize. Furthermore, the pump laser light is modeled as a continuous source rather than a one-shot switch. The excited electrons and holes recombine at a constant pace, as influenced by the interband recombination lifetime, and generate spontaneous emission, in addition to the stimulated emission induced by the input signal. Therefore, photons are being absorbed and
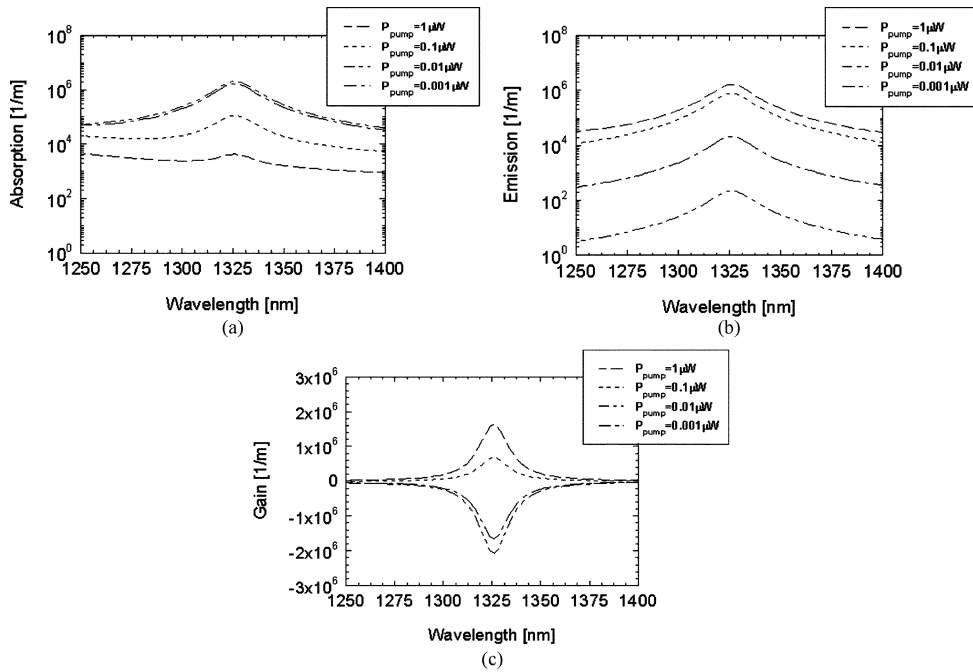
Fig. 5. (a) Absorption, (b) emission, and (c) gain spectra of a $10 \times 10 \times 10$ nm $In_{0.47}Ga_{0.53}As/InP$ quantum cube in pulsed operation.
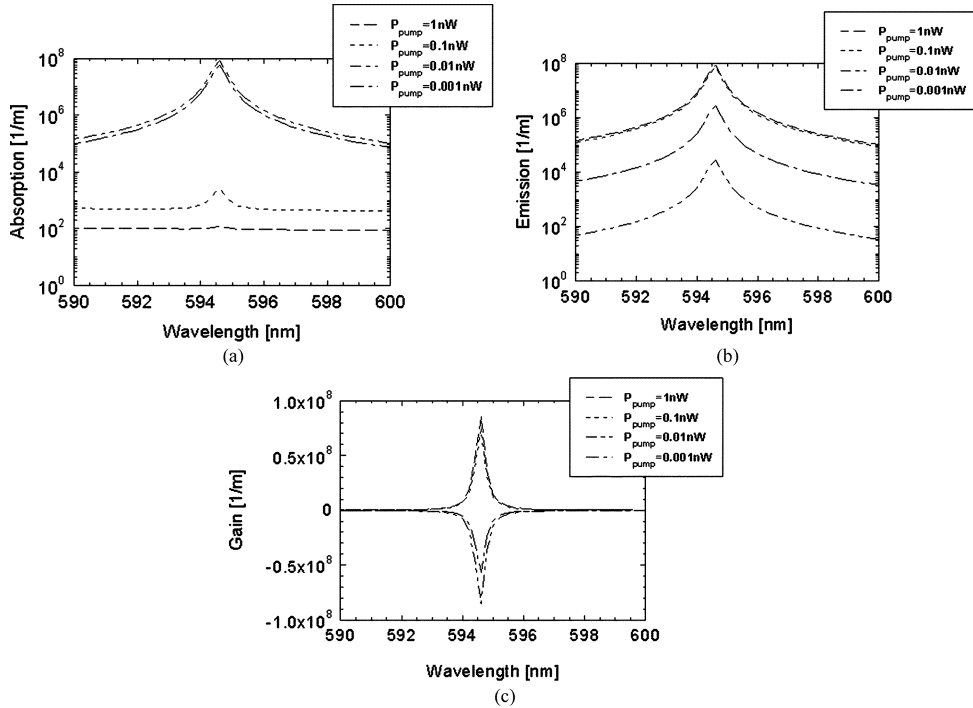

Fig. 6. (a) Absorption, (b) emission, and (c) gain spectra of a $5 \times 5 \times 5$ nm CdSe/ZnS quantum cube in pulsed operation.

emitted at a maximum rate limited by the interband recombination lifetimes.

Using a three level system under the influence of pump light, depicted in Fig. 7, we calculate the quasi-Fermi levels by considering both stimulated and spontaneous emission from the excited state. The number of electron-hole $(e^- - h^+)$ pairs at energy level 2 (denoting an electron at the first conduction band energy state and a hole at the first valence band energy state) decays through three mechanisms. 1) They can relax to energy level 1 (denoting the electron at the ground conduction band

state and hole at the ground valence band state), which happens very fast. Subsequently, the $e^- - h^+$ pairs in energy level 1 either contribute to the gain through stimulated emission by the optical signal, or spontaneously recombine to energy level 0 (denoting recombined $e^- - h^+$ pairs) at a rate specified by $r_{sp.ems,10}$ in Fig. 7. 2) At a much lower probability, $e^- - h^+$ pairs in energy level 2 can also recombine directly and create spontaneous emission at a rate of $r_{sp.ems,20}$. 3) Lastly, $e^- - h^+$ pairs may also recombine and produce stimulated emission through the aid of the pump light. Pump power affects only absorption and stimu-
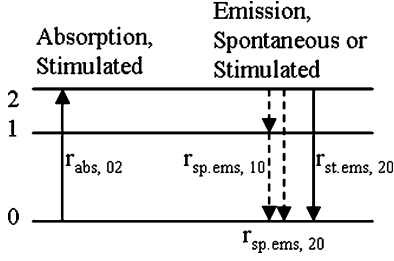
Fig. 7.   Three-level transition system.

lated emission used in the rate equation while the spontaneous emission is controlled by a decay time related to the material refractive index and excited electron energy [21]. The quasi-Fermi energy levels are determined through the simultaneous equilibrium conditions

$$N = P \Rightarrow \sum_{lmn} 2 \cdot f_c(E_{clmn})$$

$$= \sum_{lmn} 2 \cdot (1 - f_v(E_{hlmn})) \qquad (10)$$

$$r_{abs,02} = r_{st.ems,20} + r_{sp.ems,20} + r_{sp.ems,10}. \qquad (11)$$

Equation (10) is adapted from (1) and (2) with the $1/(L_x L_y L_z)$ constant factored out to signify the number of $e^- h^+$ pairs at steady state. Equation (11) depicts the equilibrium dynamics created by the pump light. Absorption and stimulated and spontaneous emission per unit time are defined as

$$r_{abs,02} = \frac{P_{pump}}{\hbar \omega_p} \alpha(\omega_p) L_z, \qquad (12)$$

$$r_{st.ems,20} = \frac{P_{pump}}{\hbar \omega_p} e(\omega_p) L_z \qquad (13)$$

$$r_{sp.ems,10} = \frac{f_c(E_{1e}) \left[1 - f_v(E_{1h})\right]}{\tau_{10}}$$

$$\times \int_{Eg}^{\infty} \frac{\frac{\hbar}{\tau_{10}}}{[E - (E_{1e} - E_{1h})]^2 + \left(\frac{\hbar}{\tau_{10}}\right)^2} dE \quad (14)$$

$$r_{sp.ems,20} = \frac{f_c(E_{2e}) \left[1 - f_v(E_{2h})\right]}{\tau_{20}}$$

$$\times \int_{Eg}^{\infty} \frac{\frac{\hbar}{\tau_{20}}}{[E - (E_{2e} - E_{2h})]^2 + \left(\frac{\hbar}{\tau_{20}}\right)^2} dE \quad (15)$$

where τ_{10} and τ_{20} represent the 1→0 and 2→0 state transition decay times.

Although (12) and (13) resemble the pulsed case formula in (7), there is no pulse duration and instead, $r_{abs,02}$ and $r_{st.ems,20}$ represent the rates at which a photon can be absorbed or emitted in the QD depending on the pump parameters. For (14) and (15), $r_{sp.ems,10}$ and $r_{sp.ems,20}$, which describe the spontaneous emission transition rates from level 1 to 0 and level 2 to 0, are shaped by the QD density of states in (5) over the whole volume. In addition, the probabilities of an electron-hole pair existing in either state 1 or 2 are described by the Fermi functions and act together as a weighting factor to the overall decay rate.

After the quasi-Fermi level energies are found by numerical analysis, the values are implemented to find the final absorp-

tion, emission and resulting gain spectra for the optical signal. Given any variation in pump power or frequency, E_{fc} and E_{fv} are recalculated to find the new gain solution. As in the pulsed case, we choose the same quantum box dimensions, the same pump energies of 1.08 and 2.45 eV and vary the pump power from 0.001 to 1 μW and 0.001 to 1 nW, respectively. The absorption, emission and gain are depicted in Fig. 8(a)–(c) for $In_{0.47}Ga_{0.53}As/InP$ and Fig. 9(a)–(c) for CdSe/ZnS.

With the two specified QD structures, saturation begins at lower pump powers for the II-VI than the III-V semiconductor compound. In a system stimulated by a CW laser, the pump parameters and the time constants associated with the material both play a role in determining the quasi-Fermi level energies. Under the steady-state condition, decreased decay times result in higher spontaneous emission rates and shorten the separation between E_{fc} and E_{fv}. Therefore, the probability of finding an electron-hole pair is reduced. For both material systems, we have approximated τ_{20} as infinity as Auger processes are thought to dominate multiple exciton events, whereas τ_{10} is set as 20 ns for CdSe/ZnS [22] and 300 ps for $In_{0.47}Ga_{0.53}As/InP$ [23]. Consequently, spontaneous emission is much higher in the latter case and lowers the amount of net excited carriers possible for the system. Furthermore, higher pump power is required to overcome the decay effects from electron-hole pair recombination to achieve saturation, which is consistent with our simulation results.

E. Gain Comparison

To determine the optimal operating region for an amplifier system, the gain coefficient, expressed as

$$\text{gain coefficient} = \frac{G(\omega)}{P_{pump}} \qquad (16)$$

is one standard for measurement [24]. In our case, QD behavior over a range of pumping powers is examined for pulsed and CW operation with the two material structures. Concentrating on the section where the curve is maximized for the input optical signal, Fig. 10 and Fig. 11 illustrate a marked difference in the results of the two optical stimulation methods.

While CdSe/ZnS moves into the positive gain from the negative (or absorption) region around 0.029 nW for pulsed and 0.014 nW for CW, $In_{0.47}Ga_{0.53}As/InP$ exhibits gain starting near 0.055 μW for pulsed and 0.008 μW for CW. The optimal pump power in a CdSe/ZnS QD is 0.055 nW for pulsed and 0.05 nW for CW. As for $In_{0.47}Ga_{0.53}As/InP$, the gain coefficient reaches a peak at 0.11 μW for pulsed and 0.019 μW for CW.

As mentioned in the pulse case analysis, smaller bandgap energies in QD materials along with larger QD dimensions lead to reduced spacing in between electron and hole states as well as lower material absorption rates. Accordingly, as evidenced in Figs. 5(c) and 6(c) as well as Figs. 8(c) and 9(c), the CdSe/ZnS system with 5-nm cube length and a larger bandgap has a higher maximum gain than $In_{0.47}Ga_{0.53}As/InP$ of 10-nm length. The Fermi energies (in Figs. 12 and 13), which shape the gain spectrum, are a manifestation of the material and pump parameter differences. In particular, E_{fc} and E_{fv} shift apart with higher
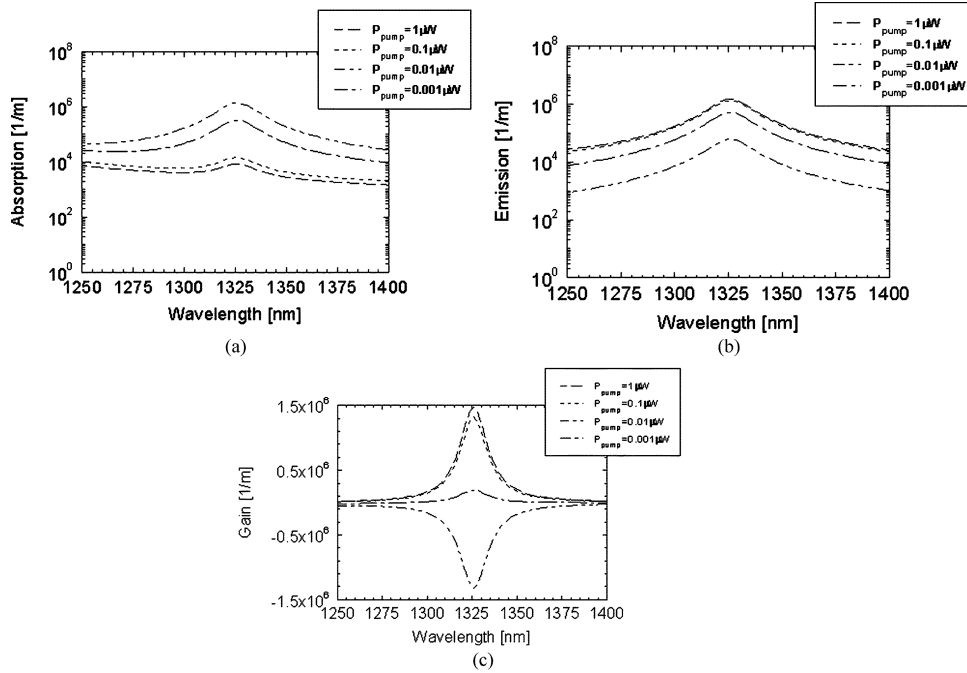
Fig. 8. (a) Absorption, (b) emission, and (c) gain spectra of a $10 \times 10 \times 10$ nm $In_{0.47}Ga_{0.53}As/InP$ quantum cube in CW operation.
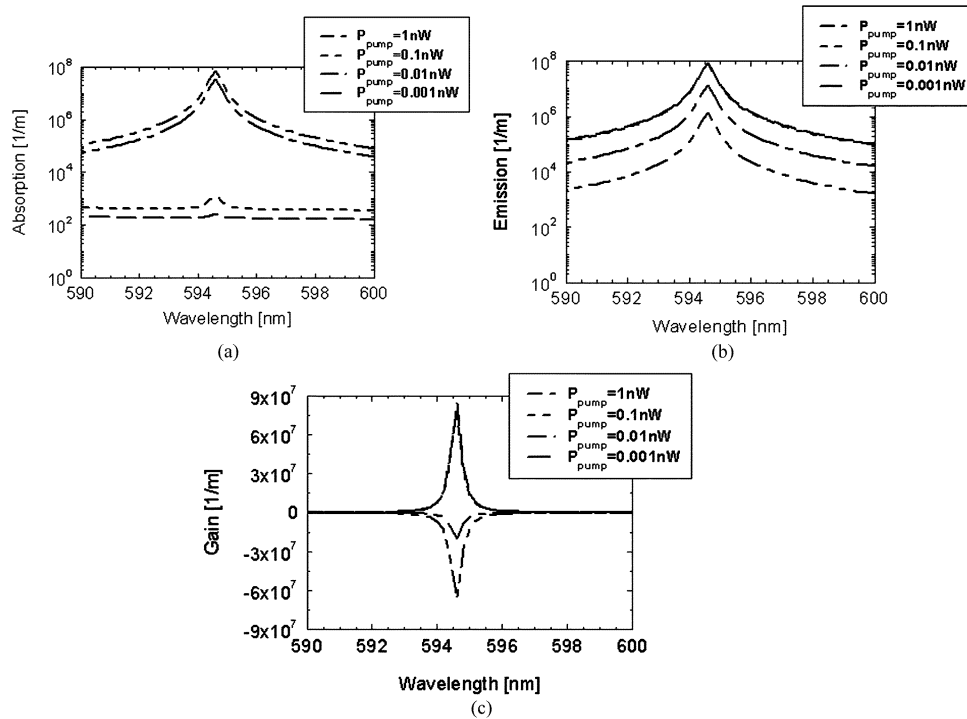

Fig. 9. (a) Absorption, (b) emission, and (c) gain spectra of a $5 \times 5 \times 5$ nm CdSe/ZnS quantum cube in CW operation.

carrier densities or additional electron or hole levels, to create the orders of magnitude difference in pump power for peak gain coefficient between the two systems.

Regarding the result that gain coefficient for CdSe/ZnS and $In_{0.47}Ga_{0.53}As/InP$ QDs both increase and the pump power necessary for net gain decreases when comparing between pulsed and CW pumping, the decay rate given by the interband recombination time, the designated pulse time, and the material constants are at the root of the trend. In other words, pulsed CdSe/ZnS requires greater pump power than CW due to the

fact that the spontaneous emission lifetime is much longer than the pump light pulse time. Similarly, compared to the pulsed case, a CW stimulated $In_{0.47}Ga_{0.53}As/InP$ QD has higher peak gain coefficient because the interband recombination time for the system is large compared to the pulse time, which allows for higher stimulated recombination rates of electron-hole pair in the first level. Equivalently, equilibrium is established with a greater number of free carriers per pump power input.

Furthermore, the gain coefficient curves are more gradual in the CW case near the optimal pump range for both QDs, and
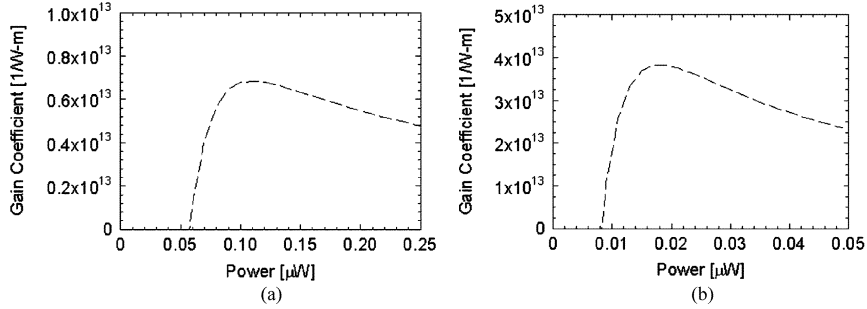
Fig. 10.   (a) Pulse and (b) CW case gain coefficients near optimal pump power for a $10 \times 10 \times 10$ nm $In_{0.47}Ga_{0.53}As/InP$ quantum cube.
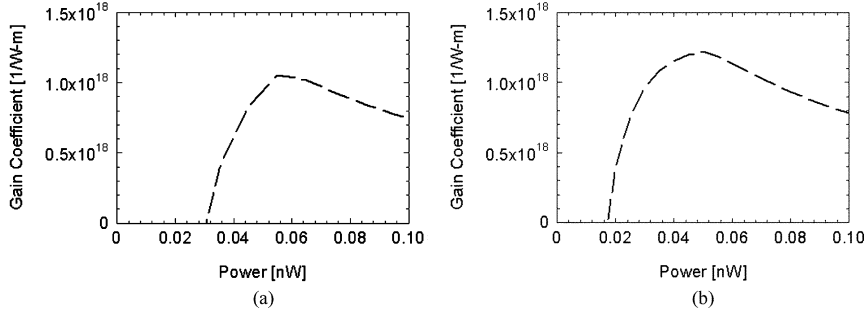
Fig. 11.   (a) Pulse and (b) CW case gain coefficients near optimal pump power for a $5 \times 5 \times 5$ nm CdSe/ZnS quantum cube.
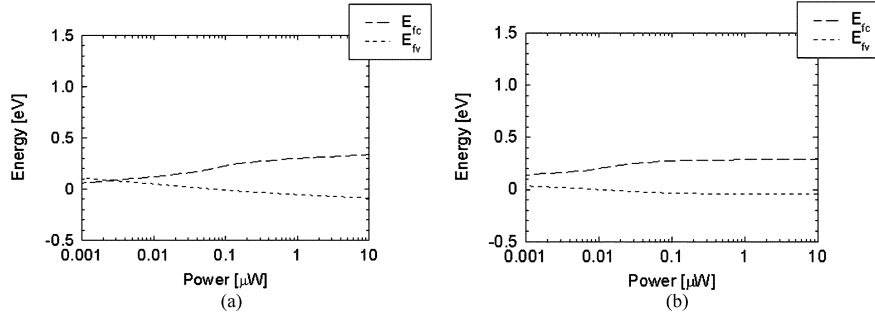
Fig. 12.   Fermi levels under (a) pulse-pumped and (b) CW-pumped for a $10 \times 10 \times 10$ nm $In_{0.47}Ga_{0.53}As/InP$ quantum cube.

are due to the smaller changes in the gain from smaller changes in the quasi-Fermi level energies under steady-state operation. In general, the shape of the gain spectrum is the same as in the pulsed case and is to be expected. Additionally, we note that full width at half maximum of the gain spectrum is on the order of 25 nm for the III-V semiconductor and about 0.5 nm for the II-VI compound, which reflects the factor of 10 disparity of the intraband relaxation times as well as the difference in bandgap energies as the lower limit for gain integration.

III. OPTICAL PROPAGATION MODELING

With the behavior under pulsed and CW optical pumping operation addressed, we now analyze the propagation characteristics given an array of QDs. The pumping laser causes the electrons to stay at the first energy level in the conduction band, from which the input signal will cause stimulated emission. The signal frequency (or wavelength) corresponds to the separation between the ground energy level in conduction band and the ground energy level in the valence band, which gives maximum

gain. Consequently, the pump and signal laser light act in combination to enable electromagnetic energy propagation in an array of QDs.

In a one-dimensional (1-D) array of QDs, the pump light shines above the waveguide while the input signal is brought incident to the edge face. As an example of a test device, we model a five QD waveguide, previously depicted in Fig. 1. At each entrance and exit face of the QD, there will be both a forward and backward propagating signals. Subsequently, traversing through the lengthwise dimension of the structure will result in signal amplification. The effect of near-field optical energy transfer between adjacent QDs [25] is modeled by assuming a coupling coefficient between the QDs. In our future work, we will model the near-field optical energy transfer process, relate the derived value to crosstalk effects between adjacent waveguides, and obtain the coupling efficiency for our device. Furthermore, the analysis will be expanded to cover two-dimensional (2-D) QD array propagation.

The intensity output at the last QD in an array of N structures may be expressed as a function of two ABCD matrices, one (M_{QD}) which describes the material, manifested through a gain
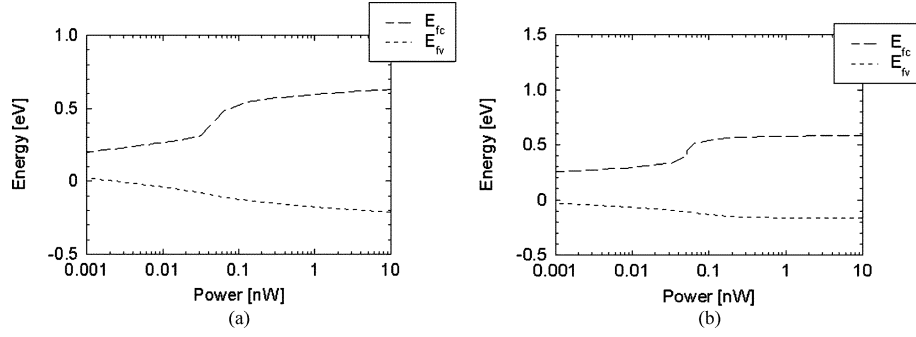
Fig. 13. Fermi levels under (a) pulse-pumped and (b) CW-pumped for a $5 \times 5 \times 5$ nm CdSe/ZnS quantum cube.
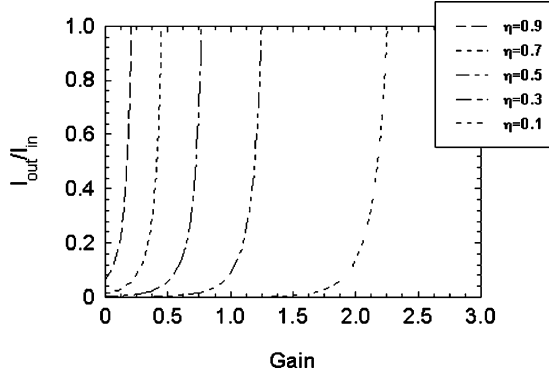

Fig. 14. Output versus input intensity as a function of gain through each QD given a range of coupling coefficients between adjacent QDs for a five QD waveguide.

value accounting for the whole length of the QD, G, and the other (M_{prop}) which uses the coupling coefficient, η, to model loss associated with the near-field optical energy transfer

$$\begin{bmatrix} I_{\text{out},+} \\ I_{\text{out},-} \end{bmatrix} = M_{QD} \cdot (M_{\text{prop}} \cdot M_{QD})^{N-1} \cdot \begin{bmatrix} I_{\text{in},+} \\ I_{\text{in},-} \end{bmatrix}, \quad \text{where}$$

$$M_{QD} = \begin{bmatrix} 0 & 1 \\ -1 & 2e^{-G} \end{bmatrix}, \text{ and } M_{\text{prop}} = \begin{bmatrix} \eta & 0 \\ 0 & \eta^{-1} \end{bmatrix}. \quad (17)$$

The "$+$" and "$-$" signs denote the forward (away from the signal source) and backward (toward the signal source) direction of travel.

To determine the relative output, or $I_{\text{out}}/I_{\text{in}}$, the multiplication from (17) is carried out such that

$$M_{\text{total}} = M_{QD} \cdot (M_{\text{prop}} \cdot M_{QD})^{N-1} = \begin{bmatrix} m_{11} & m_{12} \\ m_{21} & m_{22} \end{bmatrix}, \text{ thus,}$$

$$I_{\text{out},+} = m_{11} I_{\text{in},+} + m_{12} I_{\text{in},-},$$

$$I_{\text{out},-} = m_{21} I_{\text{in},+} + m_{22} I_{\text{in},-} \quad (18)$$

are the intensities at the last QD. Next, we apply the boundary condition $I_{\text{out},-} = 0$, which produces the solution:

$$\frac{I_{\text{out},+}}{I_{\text{in},+}} = \frac{I_{\text{out}}}{I_{\text{in}}} = m_{11} - \frac{m_{12}m_{21}}{m_{22}}. \quad (19)$$

Using the model to show the performance of a five QD waveguide Fig. 14 gives the relative intensity output plotted against the device gain over a span of coupling coefficients ($\eta = 0.1$ to 0.9), which represent reasonable and attainable values. Indeed, a η as high as 95% was reported in a nano-photonic switch system

in which energy transfer occurred across QDs of matched sizes [25].

Although the trend in Fig. 14 suggests that the intensity of the output signal can achieve very high value, realistically, in all amplified systems, the maximum output power saturates at a value determined by the material [24] as there is a finite supply of excited electrons. For illustration purposes, the maximum $I_{\text{out}}/I_{\text{in}}$ value is capped at 1 to give a reasonable demonstration range whereby larger gain requires less coupling between the QDs to achieve the same output. At higher values of η, $I_{\text{out}}/I_{\text{in}}$ rises more sharply. The simulation results also show that light propagation will be confined to the proposed waveguide with subdiffraction limit dimension, as the near-field coupling efficiency decreases rapidly when the interdot distance increases beyond a few tens of nanometers [25], which prevents crosstalk to adjacent waveguides.

IV. PROPOSED FABRICATION PROCESS

To create a QD array on a substrate that may be programmed for selective adhesion, we include DNA-linked molecules in a self-assembled process. Using compounds which chemically react with each other, layer upon layer of material is deposited, the last of which is the QDs. Then, the device may be tested by near-field coupling of a light source to the waveguide edge.

The procedure, shown in Fig. 15, begins by patterning a line via e-beam lithography on a polymethylmethacrylate (PMMA) coated oxidized silicon base. The PMMA is developed leaving a trench that opens up a silicon oxide area for surface reactions. Next, 3'mercaptopropyltrimethoxysilane (MPTMS) is added and through vapor transport, interacts, and links with the hydroxyl chains on the sample [26]. Placing drops of a buffer solution containing 5'acrylamide terminated DNA chains on the substrate, covalent bonds are formed providing a lock-and-key DNA surface attachment chemistry. Unreacted regions of MPTMS, with no oligonucleotides, are then passivated with buffered acrylic acid. Afterward, biotin modified complementary DNA strands in $2\times$ SSPE (0.3 M sodium chloride, 0.02 M sodium phosphate, 0.002 M ethylenediaminetetraacetic acid, 0.2% sodium dodecyl sulfate, pH 7.4) buffer are introduced and hybridize in the active area of the substrate [27]. Lastly, streptavidin-conjugated QDs recognize and bind to the biotin sites, and the PMMA layer is removed with toluene to yield a free standing QD waveguide.

The advantages of our fabrication process are twofold. First, the e-beam pattern generates a global QD array definition, which
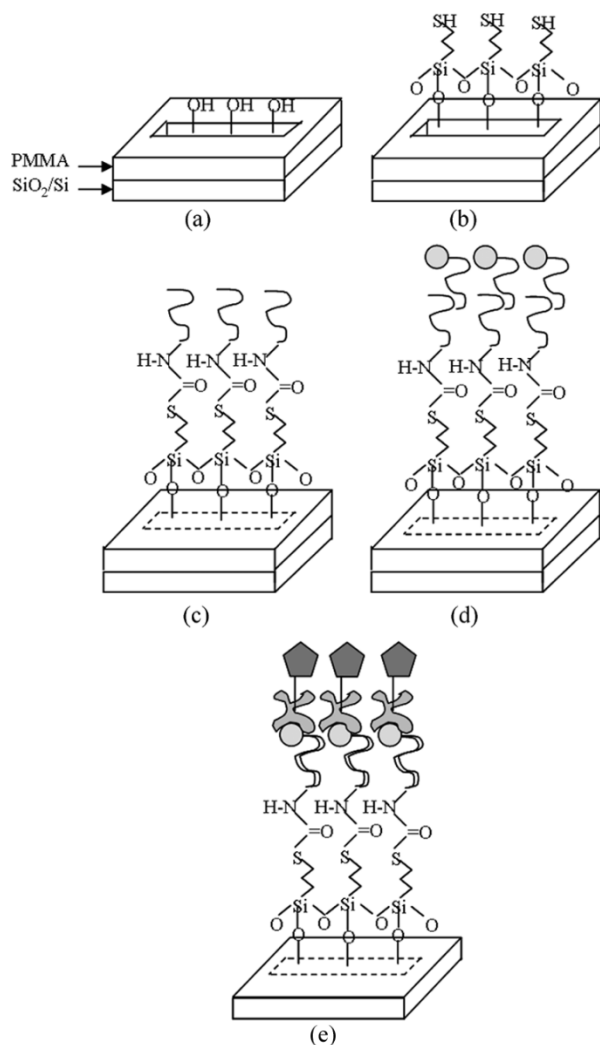
Fig. 15. Fabrication process of QD self-assembled waveguide. (a) Lines are patterned in PMMA on an oxidized silicon substrate. (b) MPTMS is added and chemisorbed. (c) 5'acrydite DNA is bound and PMMA layer is stripped. (d) Biotin modified complementary DNA strands are added. (e) QDs linked with streptavidin bind to biotin sites and become fixed to the substrate.

approaches tens of nanometers in resolution. Indeed, subdiffraction propagation is determined by the PMMA trench (or well) width and depth. Secondly, the original DNA layer enables selectivity of QD attachment to create a programmable substrate. One method which takes advantage of the DNA encoding leads to multiple QD type devices.

Specifically, the acrylamide terminated DNA chains may be deposited so that different sequences are present at separate locations. Then, each unique set of streptavidin modified QDs is mixed with corresponding biotin DNA strands of the complementary sequence. Upon adding the solutions to the substrate, the QDs will selectively adhere to the regions defined by the hybridization between matching DNA strands. Overall, the possibilities for sequential self-assembly steps involving not only QDs, but perhaps barrier materials and other desirable molecules, are countless.

V. CONCLUSION

We proposed a nano-photonic waveguide by DNA-directed self-assembled QD arrays. A theoretical model has been de-

veloped to simulate absorption, emission, and gain in optically stimulated QDs and to predict propagation characteristics for the waveguide. With a high coupling coefficient between the QDs, electromagnetic energy can be transferred with low gain values while lower coupling efficiency would require higher device gain to sustain the output intensity. On the whole, the presented models act as a foundation from which the behavior of further QD nano-photonic devices may be predicted.

Here, the QD waveguide provides the first step for the development of a photonic integrated circuit. As wires transmit information from one point to another in an electrical circuit, our photon-based waveguide may do the same, with dimensions that fall under the diffraction limit. Furthermore, QDs represent an intermediary to allow electron and photon manipulation and thus interface between the technologies. Accordingly, extensions of our work would entail exploration and modeling of QD circuits and the optical analogy to logic gates as well as applications which best capitalize on its nanometer dimension and gain properties.

REFERENCES

[1] R. Dingle and C. H. Henry, "Quantum effects in heterostructure lasers," U.S. Patent 3 982 207, Sep. 21, 1976.
[2] N. N. Ledentsov, M. Grundmann, F. Heinrichsdorff, D. Bimberg, V. M. Ustinov, A. E. Zhukov, M. V. Maximov, Z. I. Alferov, and J. A. Lott, "Quantum-dot heterostructure lasers," *IEEE J. Sel. Topics Quantum Electron.*, vol. 6, no. 3, pp. 439–451, May/Jun. 2000.
[3] V. M. Ustinov, A. E. Zhukov, A. Y. Egorov, and N. A. Maleev, *Quantum Dot Lasers*.   Oxford, U.K.: Oxford Univ. Press, 2003.
[4] W. C. W. Chan and S. Nie, "Quantum dot bioconjugates for ultrasensitive nonisotopic detection," *Science*, vol. 281, pp. 2016–2018, Sep. 1998.
[5] M. Bruchez Jr., M. Moronne, P. Gin, S. Weiss, and A. P. Alivisatos, "Semiconductor nanocrystals as fluorescent biological labels," *Science*, vol. 281, pp. 2013–2016, Sep. 1998.
[6] H. Cao, J. Y. Xu, W. H. Xiang, Y. Ma, S.-H. Chang, S. T. Ho, and G. S. Solomon, "Optically pumped InAs quantum dot microdisk lasers," *Appl. Phys. Lett.*, vol. 76, no. 24, pp. 3519–3521, Jun. 2000.
[7] O. Benson and Y. Yamamoto, "Master-equation model of a single-quantum-dot microsphere laser," *Phys. Rev. A, Gen. Phys.*, vol. 59, no. 6, pp. 4756–4763, Jun. 1999.
[8] M. Ohtsu, K. Kobayashi, T. Kawazoe, and T. Yatsui, "Nanophotonics: Design, fabrication, and operation of nanometric devices using optical near fields," *IEEE J. Sel. Topics Quantum Electron.*, vol. 8, no. 4, pp. 839–862, Jul./Aug. 2002.
[9] M. LoCascio, C. T. Ballinger, D. P. Landry, and J. E. Raynolds, "Optical Switch having a saturable absorber," U.S. Patent 6 571 028, May 27, 2003.
[10] S. G. Johnson, P. R. Villeneuve, S. Fan, and J. D. Joannopoulos, "Linear waveguides in photonic-crystal slabs," *Phys. Rev. B., Condens. Matter*, vol. 62, no. 12, pp. 8212–8222, Sep. 2000.
[11] C. A. Barrios, V. R. Almeida, R. Panepucci, and M. Lipson, "Electrooptic modulation of silicon-on-insulator submicrometer-size waveguide devices," *J. Lightw. Technol*, vol. 21, no. 10, pp. 2332–2339, Oct. 2003.
[12] J. Takahara, S. Yamagishi, H. Taki, A. Morimoto, and T. Kobayashi, "Guiding of a one-dimensional optical beam with nanometer diameter," *Opt. Lett.*, vol. 22, no. 7, pp. 475–478, Apr. 1997.
[13] M. Quinten, A. Leitner, J. R. Krenn, and F. R. Aussenegg, "Electromagnetic energy transport via linear chains of silver nanoparticles," *Opt. Lett.*, vol. 23, no. 17, pp. 1331–1333, Sep. 1998.
[14] M. L. Brongersma, J. W. Hartman, and H. A. Atwater, "Electromagnetic energy transfer and switching in nanoparticle chain arrays below the diffraction limit," *Phys. Rev. B, Condens. Matter*, vol. 62, no. 24, pp. R16356–R16359, Dec. 2000.
[15] S. A. Maier, P. G. Kik, H. A. Atwater, S. Meltzer, E. Harel, B. E. Koel, and A. A. G. Requicha, "Local detection of electromagnetic energy transport below the diffraction limit in metal nanoparticle plasmon waveguides," *Nature Mater.*, vol. 2, no. 4, pp. 229–232, Apr. 2003.

[16] C.-J. Wang, L. Y. Lin, and B. A. Parviz, "DNA-directed self-assembled waveguides for nanophotonics," presented at the *IEEE/LEOS International Optical MEMS Conf.*, Takamatsu, Japan, Aug. 22–26, 2004, Paper B5, pp. 24–25.

[17] C.-J. Wang and L. Y. Lin, "Sub-diffraction limit nano-photonic waveguides by quantum dot array structure—modeling and simulation," presented at the *SPIE Optics East Conf. Nanosensing*, Philadelphia, PA, Oct. 25–28, 2004.

[18] M. Asada, Y. Miyamoto, and Y. Suematsu, "Gain and the threshold of three-dimensional quantum-box lasers," *IEEE J. Quantum Electron.*, vol. 22, no. 9, pp. 1915–1921, Sep. 1986.

[19] K. J. Vahala, "Quantum box fabrication tolerance and size limits in semiconductors and their effect on optical gain," *IEEE J. Quantum Electron.*, vol. 24, no. 3, pp. 520–523, Mar. 1988.

[20] P. Guyot-Sionnest, M. Shim, C. Matranga, and M. Hines, "Intraband relaxation in CdSe quantum dots," *Phys. Rev. B, Condens. Matter*, vol. 60, no. 4, pp. R2181–R2184, Jul. 1999.

[21] P. Bhattacharya, *Semiconductor Optoelectronic Devices*, 2nd ed. Englewood Cliffs, NJ: Prentice-Hall, 1996, pp. 220–221.

[22] B. R. Fisher, H.-J. Eisler, N. E. Stott, and M. G. Bawendi, "Emission intensity dependence and single-exponential behavior in single colloidal quantum dot fluorescence lifetimes," *J. Phys. Chem. B*, vol. 108, pp. 143–148, Jan. 2004.

[23] M. Petrauskas, S. Juodkazis, V. Netikis, M. Willander, A. Ouacha, and B. Hammarlund, "Picosecond carrier dynamics in highly excited InGaAs/InP/InGaAsP/InP structures," *Semiconduct. Sci. Technol.*, vol. 7, pp. 1355–1358, Nov. 1992.

[24] C. R. Giles and E. Desurvire, "Modeling erbium-doped fiber amplifiers," *J. Lightw. Technol.*, vol. 9, no. 2, pp. 271–283, Feb. 1991.

[25] T. Kawazoe, K. Kobayashi, S. Sangu, and M. Ohtsu, "Demonstrating nanophotonic switching using near-field pump-probe photoluminescence spectroscopy of CuCl quantum cubes," *J. Microsc.*, vol. 209, pp. 261–266, Mar. 2003.

[26] D. G. Kurth and T. Bein, "Surface-reactions on thin-layers of silane coupling agents," *Langmuir*, vol. 9, no. 11, pp. 2965–2973, Nov. 1993.

[27] L. M. Demers, D. S. Ginger, S.-J. Park, Z. Li, S.-W. Chung, and C. A. Mirkin, "Direct patterning of modified oligonucleotides on metals and insulators by dip-pen nanolithography," *Science*, vol. 296, pp. 1836–1838, Jun. 2002.

Chia-Jean Wang (S'04) received the B.S. degree (with honors) in electrical engineering from the California Institute of Technology (Caltech), Pasadena, in 2001, and the M.S. degree in 2004 from the University of Washington, Seattle, where she is currently working toward the Ph.D. degree.

From 2001 to 2003, she was a Member of the Technical Staff with the Photonics Section at Northrop Grumman Space Technology (formerly TRW), Redondo Beach, CA. During the summers of 1998 and 2000, she interned in the Fluid and Thermodynamics and Avionics groups at TRW, respectively. In 2000, she was a Richter Fellow of the Summer Undergraduate Research Fellowship program at Caltech, where she was exploring evolvable hardware platforms. Her current interests include investigating quantum dot models and applications.

Ms. Wang is the recipient of the Boeing Fellowship for 2003–2004, and the NSF Graduate Fellowship, on tenure for 2003–2006.

Lih Y. Lin (M'94–SM'02) received the Ph.D. degree in electrical engineering (with highest honors) from the University of California, Los Angeles, in 1996. Her doctoral research focused on high-speed photonics and micromachined integrated optics.

After receiving her degree, she joined AT&T Labs-Research, Red Bank, NJ, where she conducted research on micromachined technologies for optical switching and lightwave systems. In March 2000, she joined Tellium, Inc., Oceanport, NJ, as Director of Optical Technologies. She has been an Associate Professor with the Electrical Engineering Department, University of Washington, Seattle, since June 2003. She has served on the technical program committee and co-chaired various technical conferences, including International Optical MEMS Conference, CLEO Pacific Rim, IEEE LEOS Annual Meeting, OSA Annual Meeting, and OSA Photonics in Switching Topical Meeting. Currently, she is on the steering committee of the International Optical MEMS Conference. She has over 120 publications in refereed journals and conferences. She holds 21 U.S. patents, and has seven patents pending. Her current research interests include nano-photonics and optical MEMS.

Dr. Lin was the editor for JOURNAL OF LIGHTWAVE TECHNOLOGY: Special Issue on Optical MEMS and its Future Trends. She was a Finalist of the 2001 IEEE Eta Kappa Nu Outstanding Young Electrical Engineer Award, and she received the MIT Technology Review 100 Award in 2003.

Babak A. Parviz (S'94–M'01) received the B.S. degree in electrical engineering from Sharif University of Technology, in 1995, and the M.S. degree in electrical engineering, the M.S. degree in physics, and the Ph.D. degree in electrical engineering from the University of Michigan, Ann Arbor, in 1997 and 2001, respectively.

From 2000 to 2001, he was with Nanovation Technologies Inc., Evanston, IL, as a Device Designer and Product Manager for integrated optical MEMS devices. From 2001 to 2003, he was a Postdoctoral Research Fellow with the Department of Chemistry and Chemical Biology, Harvard University, Cambridge, MA. He joined the Electrical Engineering Department, University of Washington, Seattle, as an Assistant Professor in October 2003. His research interests include self-assembly, nano- and microfabrication, organic/molecular electronics and photonics, bioMEMS, and nanomedicine.

Dr. Parviz is a member of the American Association for Advancement of Science, Sigma Xi, and the American Chemical Society. He received the Distinguished Achievement Award from the Electrical Engineering Department of the University of Michigan, Bronze Medal from the 22nd International Physics Olympiad, and the First Prize of the Kharazmi Award.